Genetic algorithm prediction of two-dimensional group-IV dioxides for dielectrics

Arunima K. Singh, Benjamin C. Revard, Rohit Ramanathan, Michael Ashton, Francesca Tavazza, and Richard G. Hennig

Genetic Algorithm Prediction of Two-Dimensional Group-IV Dioxides for Dielectrics

Arunima K. Singh,[1,2] Benjamin C. Revard,[3,4] Rohit Ramanathan,[3]
Michael Ashton,[4] Francesca Tavazza,[1] and Richard G. Hennig[4,3]

[1] *Materials Science and Engineering Division, National Institute of Standards and Technology, Gaithersburg, MD 20899, U.S.A.*
[2] *Energy Technologies Area, Lawrence Berkeley National Laboratory, Berkeley, CA 94720, U.S.A*
[3] *Department of Materials Science and Engineering, Cornell University, Ithaca, NY 14850, U.S.A.*
[4] *Department of Materials Science and Engineering,*
University of Florida, Gainesville, FL 32611, U.S.A.

Two-dimensional (2D) materials present a new class of materials whose structures and properties can differ from their bulk counterparts. We perform a genetic algorithm structure search using density-functional theory to identify low-energy structures of 2D group-IV dioxides AO_2 (A=Si, Ge, Sn, Pb). We find that 2D SiO_2 is most stable in the experimentally determined bi-tetrahedral structure, while 2D SnO_2 and PbO_2 are most stable in the $1T$ structure. For 2D GeO_2, the genetic algorithm finds a new low-energy 2D structure with monoclinic symmetry. Each system exhibits 2D structures with formation energies ranging from 26 to 151 meV/atom, below those of certain already synthesized 2D materials. The phonon spectra confirm their dynamic stability. Using the HSE06 hybrid functional, we determine that the 2D dioxides are insulators or semiconductors, with a direct band gap of 7.2 eV at Γ for 2D SiO_2, and indirect band gaps of 4.8 - 2.7 eV for the other dioxides. To guide future applications of these 2D materials in nano-electronic devices, we determine their band-edge alignment with graphene, phosphorene, and single-layer BN and MoS_2. An assessment of the dielectric properties and electrochemical stability of the 2D group-IV dioxides shows that 2D GeO_2 and SnO_2 are particularly promising candidates for gate oxides and SnO_2 also as a protective layer in heterostructure nanoelectronic devices.

I. INTRODUCTION

Two-dimensional (2D) crystalline materials exhibit a periodic structure in two dimensions and a finite extent in the third dimension.[1–3] These materials are of great interest as they maximize their surface area, display large quantum confinement, and exhibit different symmetries compared to their bulk counterparts.[1,4] Quantum confinement generally increases the band gap of 2D materials compared to corresponding bulk materials.[1,4] This leads, for example, to increased photocatalytic activity in 2D SnS_2 compared to the bulk material[5,6] and enhanced photoluminescence in single-layer MoS_2 due to its direct band gap.[7,8] Several non-piezoelectric bulk materials lose their inversion symmetry when reduced to 2D form and thus become piezoelectric.[9–11] As a consequence, 2D materials potentially have a wide variety of applications in opto-electronic devices, sensing applications, and energy conversion technologies.[12–14]

Many materials systems exhibit metastable 2D phases. Computational techniques such as density-functional theory (DFT) offer a way to rapidly determine the stability of hypothetical 2D materials and characterize their properties to identify potentially useful 2D phases. As an example, DFT previously predicted the 2D phase of GaN and its stability and structural relaxation on various substrates.[15–17] Recently, 2D GaN was synthesized in experiments and shown to exhibit the predicted buckled structure.[18]

A key step in the discovery of 2D materials is structure determination. A common technique for identifying the structure of a 2D material is to isolate a slab from a low energy plane of the material's bulk structure.[1,19]
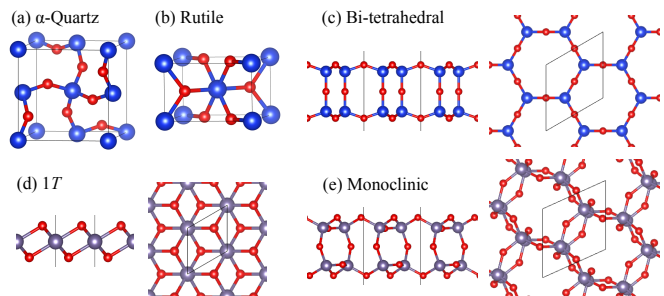
FIG. 1. Bulk crystal structure of (a) α-quartz and (b) rutile structure of SiO_2 and 2D structures of (c) bi-tetrahedral SiO_2, (d) $1T$ AO_2 (A = Ge, Sn, Pb) and (e) monoclinic structure of GeO_2.

This approach works very well for materials with layered structural motifs, such as van der Waals bonded layered materials, where the 2D structure is often just a single layer of the bulk phase, but it fails for a material such as SiO_2, which has recently been synthesized in both crystalline and amorphous 2D forms.[20–22] Figs. 1 (a) and (c) show that the structure of 2D SiO_2 is fundamentally different from that of α-quartz.[22]

In this work, we identify the low-energy 2D structures of group-IV dioxides using the Genetic Algorithm for Structure Prediction (GASP) code.[3,23,24] Coupled with accurate DFT methods, GASP efficiently explores a material's multidimensional potential energy surface. GASP has been successfully applied to predict low-energy structures for various bulk and 2D systems including In-P, Sn-S and C-Si.[3,25,26] We show that the 2D group-IV dioxides AO_2 (A = Ge, Sn, Pb) exhibit monoclinic and $1T$ struc-
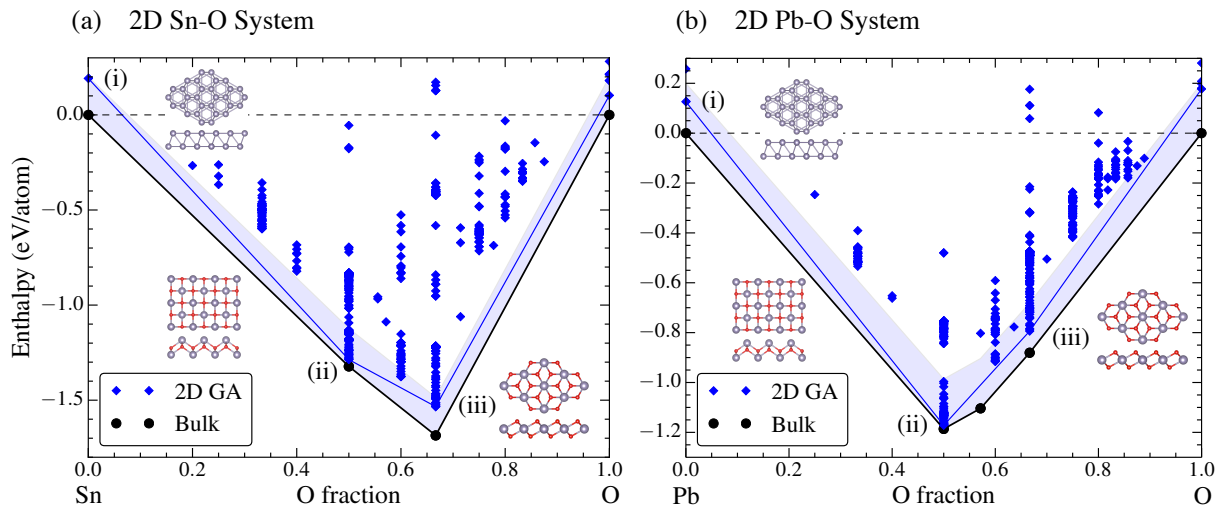
FIG. 2. 2D structure searches for the (a) Sn-O and (b) Pb-O systems. The black circles denote the ground state bulk structures, and the lines connecting them form the bulk convex hull. The light blue shading indicates the region less than 200 meV/atom above the bulk convex hull. The blue diamonds denote 2D structures found by the genetic algorithm, and the blue line segments form the convex hull for the 2D structures. The algorithm found the same three low-energy structures on the 2D convex hull of each system, shown in each plot and labeled (i) - (iii).

tures with low formation energies relative to competing bulk phases. The phonon spectra confirm their dynamic stability. We find that the 2D dioxides are insulators or large-gap semiconductors with favorable band offsets to common 2D materials, exhibit a high permittivity, and are stable in aqueous environments, indicating their potential for application as dielectrics and protective layers in nanoelectronics.

Figs. 1(a) and (b) show the ground state bulk structures of the group-IV dioxides. The thermodynamically stable phase for bulk SiO_2 is α-quartz (space group $P3_221$),[27] while GeO_2, SnO_2, and PbO_2 occur in the rutile structure (space group $P4_2/mn$).[28,29] In α-quartz, Si is four-fold and O two-fold coordinated. In the rutile phase, the cations are six-fold and O is three-fold coordinated.

II. METHODS

A. Density-Functional Calculations

We employ the Vienna Ab-initio Simulation Package (VASP)[30–33] for all DFT calculations using the projector augmented wave (PAW) method.[34] The structural relaxations are performed with the Perdew-Burke-Ernzerhof (PBE) generalized-gradient exchange-correlation functional.[35] A plane-wave energy cutoff of 500 eV and a k-point mesh density of 30 per Å^{-1} ensures convergence of the energy to 1 meV/atom. For the 2D materials, a vacuum spacing of 10 Å reduces the interaction between layers to about 1 meV/atom. To accurately determine the electronic properties of the 2D materials, we use the Heyd-Scuseria-Ernzerhof (HSE06)

hybrid functional[36] with a k-point mesh density of 40 per Å^{-1} for all the materials except graphene and phosphorene, which require meshes of 95 and 115 k-points per Å^{-1}, respectively. The phonon spectra are calculated from the force constants using the PHONOPY package.[37] The force constant for a $4 \times 4 \times 1$ supercell are obtained with density functional perturbation theory for SnO_2 and PbO_2 with 3 atoms in the primitive cell and the finite displacement method for the experimentally observed SiO_2 bi-tetrahedral structure with 12 atoms in the primitive cell.[38]

B. 2D Structure Search

We use the genetic algorithm for structure and phase prediction (GASP)[3,23] to identify the low-energy 2D structures of the AO_2 compounds (A = Si, Ge, Sn, Pb). The genetic algorithm starts with an initial population of random structures that broadly samples the solution space. The structures are relaxed and low-energy structures are preferentially selected as parents to create child structures using genetic operators such as mutation and mating. When enough child structures have been created, they in turn are selected to make offsprings of their own. This process continues until some user-defined stopping criteria are met. The GASP code is freely available under the GPL v3 license at https://github.com/henniggroup.

In the 2D structure searches, the number of atoms is allowed to vary, and we use an upper limit of 15 atoms per cell. The layer thickness of the 2D materials is constrained to 4 Å. For the Sn-O and Pb-O systems, we employ the phase diagram searching mode of the algo-
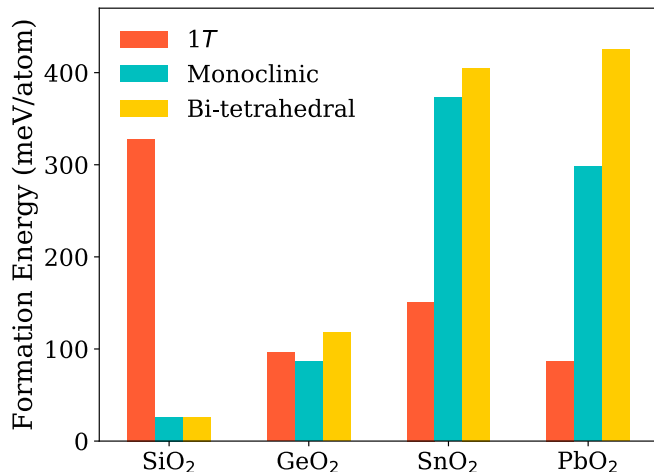
FIG. 3. Formation energies of the $1T$, bi-tetrahedral and monoclinic 2D structures for SiO_2, GeO_2, SnO_2 and PbO_2.

rithm, which allows the stoichiometry to vary, and we stop the searches after 1000 structure relaxations. For the 2D SiO_2 and GeO_2 searches, we fix the stoichiometry and use a stopping criterion of 500 structure relaxations.

For the 2D SiO_2 and GeO_2 system we perform secondary structure searches in which the initial population is seeded with the bi-tetrahedral structure, as well as the low-energy structures found in the first searches. For the second GeO_2 search, we also seeded the initial population with the low-energy structures found in the second SiO_2 search. We impose a more liberal layer thickness constraint of 6 Å for these secondary searches, and to speed up the structural relaxations, we use the default cutoff energies and a k-point mesh density of only 20 per $Å^{-1}$. We then re-relax the best third of the resulting structures with the converged parameters (500 eV cutoff energy and 30 per $Å^{-1}$ k-point mesh density).

III. RESULTS

A. 2D Structure Prediction

Fig. 2 shows the energies of the 2D structures found by the genetic algorithm in the Sn-O and Pb-O binary systems relative to the ground state structures of bulk Sn or bulk Pb, respectively, and O_2. The genetic algorithm identifies the same three structures on the 2D convex hulls in both systems: (i) the high buckled hexagonal Sn and Pb structure, which was previously reported,[40] (ii) the tetragonal litharge structure, which was previously predicted for both SnO and PbO,[41] and (iii) the $1T$ structure, which is the lowest energy structure of several other 2D dichalcogenides, such as 2D SnS_2,[42] but not yet reported for 2D oxides.

In the first 2D GeO_2 structure search, the algorithm finds the $1T$ structure to have the lowest energy, Fig 1 (d). However, in the second search, in which the initial

population is seeded with the bi-tetrahedral and other low-energy structures, the algorithm finds a lower energy structure with monoclinic symmetry, shown in Fig. 1(e). Some other low energy GeO_2 structures with energies only slightly larger than that of the monoclinic structure are also identified, however, the phonon dispersion of these structures reveals that they are dynamically unstable (see supplementary materials).

Similarly, in the first 2D SiO_2 search, the lowest energy structure found by the algorithm is not the experimentally observed bi-tetrahedral structure, but rather an orthorhombic structure with higher energy (see supplementary materials). In the second, seeded search, the algorithm uncovers two other low-energy 2D SiO_2 structures, that are energetically unfavorable compared to the bi-tetrahedral structure and are also dynamically unstable (see supplementary materials).

As mentioned above, the genetic algorithm did not succeed in finding the lowest energy 2D structures of SiO_2 and GeO_2 in the first searches. We speculate that due to their open character, these structures pose a difficult challenge for the genetic algorithm. In particular, it is unlikely for features as large as the open vacuum regions in the bi-tetrahedral structure, which have a diameter of about 6 Å, to appear in randomly generated structures because the fractional atomic coordinates are drawn from a uniform distribution. Furthermore, such a large irreducible feature will probably not arise in the subsequent population. The genetic operators work by combining and perturbing local structural motifs of parents to create offspring, so if no parent structure contains a particular irreducible trait, it is unlikely to appear in the offspring.

We have shown that if prior knowledge about the system of interest is available, it can be used to overcome the difficulty of finding structures with large irreducible features by seeding the initial population with known structures possessing those features.

B. Energetic and Dynamic Stability

We examine the energetic stability of all 2D group-IV dioxides, SiO_2, GeO_2, SnO_2 and PbO_2, in the two low-energy 2D structures discovered by the genetic algorithm, $1T$ and monoclinic, and the experimental bi-tetrahedral SiO_2 structure by comparing their formation energies relative to the competing bulk phases, $\Delta E^f = E_{2D}/N_{2D} - E_{3D}/N_{3D}$, where E and N are the energies of and numbers of atoms in the respective phases. Fig. 3 illustrates the computed formation energies of these 2D materials. We note that the lowest energy structure of 2D SiO_2 is the experimental bi-tetrahedral structure. The lowest energy structure of GeO_2 is the monoclinic structure and that of SnO_2 and PbO_2 is the $1T$ structure, both found by the genetic algorithm. In the monoclinic structure, Ge is four-fold coordinated, unlike the bulk rutile structure, which is six-fold coordinated. For the

TABLE I. Structure information, including lattice parameter, a and b, space group, and Wyckoff positions, formation energy, ΔE_f, and cation Bader charge, Q for the 2D group-IV dioxide structures. We have used 3D space groups to describe these finite-thickness 2D structures that lack periodicity in the direction normal to the 2D sheet. In the representations given here, the $\vec{c}$ lattice vector is normal to the plane of the 2D sheet. The vertical components of the general Wyckoff positions are given as distances from the mirror plane, and the in-plane components are given as fractions of the $\vec{a}$ and $\vec{b}$ lattice vectors. Symmetry information was obtained with the FINDSYM software package.[39]

	Space group	a, b (Å)	γ (°)	Atomic positions	ΔE_f (meV/atom)	Q (e)
Bi-tetrahedral SiO$_2$	$P6/mmm$ (191)	5.325, 5.325	120.0	Si 4(h) $z = 1.627$ Å	26	3.22
				O 2(d); O 6(i) $z = 2.162$ Å		
Monoclinic GeO$_2$	$C2/m$ (12)	5.746, 8.897	90.0	Ge 8(j) $x = 0.529$, $y = 0.189$, $z = -1.620$ Å	86	2.23
				O 4(h) $y = 0.775$; O 4(i) $x = 0.372$, $z = 1.533$ Å		
				O 8(j) $x = 0.757$, $y = 0.290$, $z = 2.477$ Å		
$1T$ SnO$_2$	$P\bar{3}m1$ (164)	3.225, 3.225	120.0	Sn 1(b); O 2(d) $z = 1.015$ Å	151	2.22
$1T$ PbO$_2$	$P\bar{3}m1$ (164)	3.408, 3.408	120.0	Pb 1(b); O 2(d) $z = 1.075$ Å	87	1.74
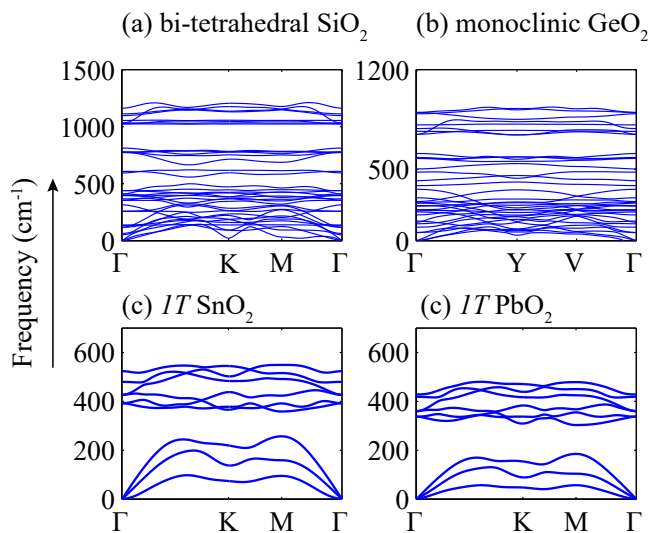
FIG. 4. Phonon dispersion curves for (a) bi-tetrahedral SiO$_2$, (b) monoclinic GeO$_2$, (c) 1T SnO$_2$, and (d) 1T PbO$_2$. The lack of unstable modes demonstrates the dynamic stability of these four 2D materials.

other group-IV dioxides, the coordination of the cations in the lowest-energy 2D structures is the same as in their bulk counterparts.

Table I summarizes the formation energies and structural parameters of the lowest energy 2D structure of each dioxide. The monoclinic structure of GeO$_2$ and the 1T structures of SnO$_2$ and PbO$_2$ all have formation energies below 200 meV/atom, similar to those of already extant two-dimensional materials.[2,3] This indicates promise for experimental synthesis of 2D GeO$_2$, SnO$_2$ and PbO$_2$ as free-standing films.

In addition, the lack of imaginary modes in the phonon spectra in Fig. 4 confirms that all the structures are dynamically stable. The highest frequency of the optical modes decreases with increasing mass of the cation. The significantly harder longitudinal optical modes in 2D

SiO$_2$ and monoclinic GeO$_2$ indicates that they have a higher in-plane rigidity in comparison to the 1T 2D structures of AO$_2$ (A = Ge, Sn, and Pb).

C. Electronic Properties

We next examine the electronic properties of the 2D dioxides with the HSE06 hybrid functional, which has been shown to give band gaps in good agreement with experimental values.[2,43] Fig. 5 shows the band structure projected onto the oxygen atoms for the four 2D dioxides. All of the 2D dioxides except PbO$_2$ are insulators, see Tab. II. The bi-tetrahedral SiO$_2$ exhibits a direct band gap at the Γ-point, while the monoclinic GeO$_2$ and the 1T structures of SnO$_2$ and PbO$_2$ display indirect gaps. The conduction band minimum (CBm) is at the gamma point for all 2D dioxides. The band gap of the 2D dioxides decreases with increasing cation size, similar to the measured band gaps of the bulk dioxides.[44–46] The decrease in band gap across the cation series corresponds with a decrease in ionicity of the bonds, as measured by the Bader charge shown in Tab. I. [Singh: Please verify that the Bader charges follow the trend.]

The oxygen-projected band structures show that the

TABLE II. Electronic band gap, E_{2D}^{HSE06} in eV, in-plane and out-of-plane permittivity components, ϵ_{11}, ϵ_{22} and ϵ_{33}, and exciton binding energy, E_{exc} in eV, estimated from the Mott-Wannier model, for the group-IV dioxides. The experimentally measured band gaps, E_{bulk}^{exp}, of the bulk phases are also listed.[44]

	E_{2D}^{HSE06}	E_{bulk}^{exp}	ϵ_{11}^{2D}	ϵ_{22}^{2D}	ϵ_{33}^{2D}	E_{exc}
Bi-tet SiO$_2$	7.20	10.4, 11	2.6	2.6	2.0	3.0
Monoclinic GeO$_2$	4.81	5.54, 5.56	3.6	3.4	2.1	1.6
1T SnO$_2$	4.09	2.45-4.1	5.9	5.9	2.2	0.9
1T PbO$_2$	2.65	1.4, 1.5	7.9	7.9	2.3	0.9
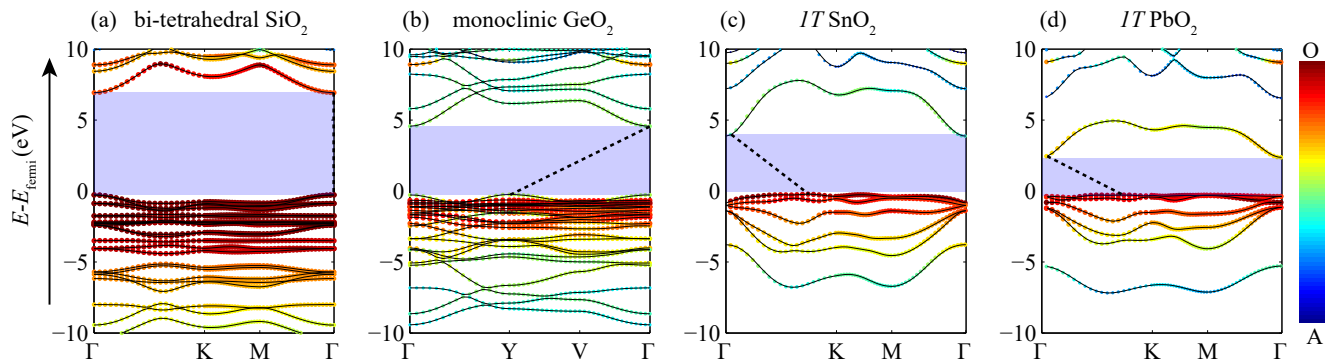
FIG. 5. Projected electronic band structure of (a) bi-tetrahedral SiO$_2$, (b) monoclinic GeO$_2$, (c) 1T SnO$_2$, and (d) 1T PbO$_2$. The symbol sizes and colors denote the weights of group-IV elements, A, and O atoms. The lowest energy band transitions are shown by dashed lines.

valence band maxima (VBM) are dominated in all compounds by oxygen p states. In the 2D SiO$_2$ structure, the CBm states are dominated by the empty 4s states of silicon and 3s states of oxygen with the empty Si 3p states at slightly higher energy. In the monoclinic GeO$_2$ structure, the CBm has contributions from the empty group-IV atom s orbitals and the O s and p orbitals. In the other 2D oxides with the 1T structure, the CBm has a different characteristic. Apart from the CBm being dominated by group-IV atom s and O p orbitals, there are contributions from the hybridized spd orbitals of the group-IV atoms.

To determine if the 2D group-IV dioxides could be useful as gate oxides in electronic devices, we compare in Fig. 6 the band edge positions determined with the HSE06 functional for the 2D dioxides with four common 2D materials - graphene, phosphorene, single-layer MoS$_2$, and single-layer BN. Band offsets exceeding 1 eV are desirable between gate oxides and semiconductors in electronic devices as this causes low leakage current due to Schottky emissions.[47] We observe that the CBm energy of the dioxides decreases rapidly with cation size, while the VBM remains largely unchanged. We find that 2D SiO$_2$ can serve as an excellent gate oxide for MoS$_2$ and phosphorene with band offsets well above 1 eV. In comparison, single-layer BN is more suitable for phosphorene and graphene. Single-layer BN is expected to cause larger leakage currents for single-layer MoS2$_2$ due to the small offset of 0.24 eV in the VBM of BN and MoS$_2$. The band offsets between 2D SiO$_2$ and MoS$_2$ are 2.17 and 2.89 eV for the CBm and VBM, respectively and between 2D SiO$_2$ and phosphorene they are 1.74 and 3.85 eV, respectively.

The other 2D dioxides studied in this work are not predicted to be suitable as a gate oxide for MoS$_2$ and phosphorene. However, non-epitaxial heterostructures of type-II are possible for SiO$_2$/BN, GeO$_2$/MoS$_2$, GeO$_2$/BN, GeO$_2$/phosphorene, SnO$_2$/BN, SnO$_2$/MoS$_2$, SnO$_2$/phosphorene and type III-heterostructure are possible for PbO$_2$/MoS$_2$, PbO$_2$/BN and PbO$_2$/phosphorene. In type-II heterostructures, it
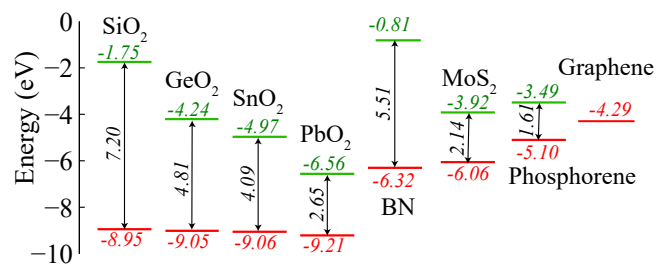
FIG. 6. The HSE06 band edge alignment of 2D group-IV dioxides in comparison to that of single-layer BN, single-layer MoS$_2$, phosphorene and graphene.

is expected that the free electrons and holes will spontaneously separate into the different layers, which is useful for optoelectronics and solar energy conversion.[48]

Next, we compute the static permittivity tensors of the 2D group-IV dioxides, single-layer MoS$_2$ and phosphorene.[49] The dioxides and MoS$_2$ in the hexagonal symmetry have two independent permittivity tensor elements, $\epsilon_{11} = \epsilon_{22}$ and ϵ_{33}. The 2D structures with monoclinic and orthorhombic symmetries, including phosperene, have three independent tensor elements, ϵ_{11}, ϵ_{22} and ϵ_{33}. A k-point mesh of $16 \times 16 \times 1$ leads to a convergence of the tensor elements to better than the first decimal place. To account for the contribution of the vacuum to the computed permittivity tensor elements, ϵ^{calc}, we use the linear law,[42,50] $\epsilon^{calc} = f \epsilon^{2D} + (1 - f) \epsilon^{vac}$, where f is the volume fraction of the 2D structures in the simulation cell assumed as the sum of the maximum distance between the farthest atoms in the direction perpendicular to the plane of the 2D materials and the atomic radii[51] of the farthest atoms, $\epsilon^{vac} = 1$ is the permittivity of vacuum and ϵ^{2D} is the permitivitty of the 2D materials.

Table II shows the permittivity tensor components of the 2D structures obtained by assuming the thickness of the 2D materials as the sum of the maximum distance between the farthest atoms in the direction perpendicular to
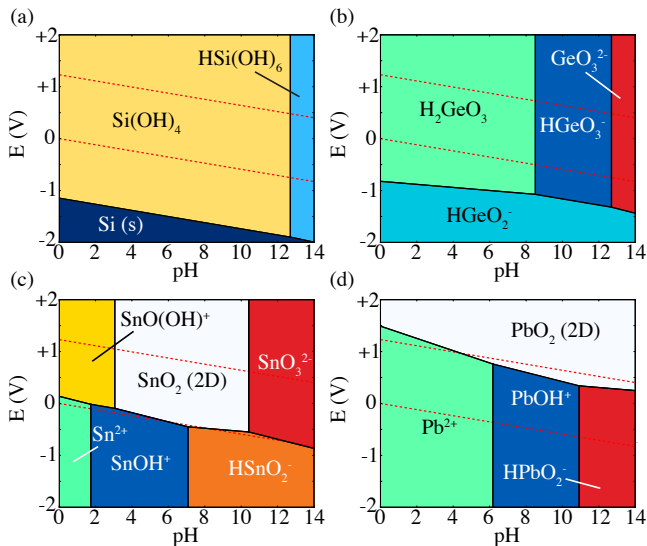
FIG. 7. Environmental stability of the 2D group-IV dioxides. The Pourbaix diagrams of (a) 2D SiO_2 in the bi-tetrahedral or orthorhombic structure and (b) 2D GeO_2 in the $1T$ or orthorhombic structure show that these compounds are thermodynamically unstable in water. In contrast, (c) $1T$ SnO_2 and (d) $1T$ PbO_2 exhibit a large window of stability. The Pourbaix diagrams are drawn for ionic concentrations of 10^{-6} M.

to the plane of the 2D materials and the atomic radii[51] of the farthest atoms. The first exciton binding energies, E_{exc}, estimated from the Mott-Wannier model[42,52] are also listed. The smaller energy gap materials yield larger dielectric constants, which can be explained by the Penn model,[53] $\epsilon \approx 1 + (\frac{\hbar \omega_p}{E_g})^2$, where ω_p is the plasma frequency and E_g is the band gap. A comparison of the permittivity of the 2D group-IV dioxides, single-layer MoS_2 and phosphorene, and the stable bulk phases corresponding to them[54–60] can be found in the supplementary material. With their high permittivity, 2D GeO_2, SnO_2 and PbO_2 are potential candidates for replacing amorphous SiO_2 with ϵ=3.9,[61] as gate oxides in nanoelectronic applications.

D. Environmental Stability

To determine if the 2D dioxides could, in addition to being a gate oxide, also provide protection of the active semiconducting layers from environmental degradation, we calculate their Pourbaix diagrams. Fig. 7 compares the stability of the 2D dioxides in aqueous environment as a function of applied potential and pH for an ionic concentration of 10^{-6} M. Similar to their bulk counterparts, the 2D dioxides of Sn and Pb provide a large window of thermodynamic stability, while the 2D dioxides of Si and Ge are thermodynamically unstable over all or most of the accessible range of pH and voltage, and up to ionic concentrations of 1M. The Pourbaix diagrams of 2D SiO_2

and GeO_2 resemble those of the bulk phases, with comparably poor stability in an aqueous environment. However, for SiO_2, the sufficiently high concentrations of silicon hydroxide usually present in water and slow dissolution kinetics lead to the observed environmental stability of the various polymorphs of SiO_2.[62,63] We therefore expect that 2D SiO_2 exhibits a similar enhanced kinetic stability and may be useful as a protective layer for various applications. On the other hand, the predicted excellent environmental stability and high permittivity of 2D SnO_2 and PbO_2 make these two materials ideal candidates for gate oxides and protective layers in nanoelectronic devices.

IV. CONCLUSION

In summary, we have used a genetic algorithm for structure prediction coupled with density functional theory calculations to identify the structures of the 2D group-IV dioxides. We confirm that 2D SiO_2 is most stable in its experimentally determined bi-tetrahedral structure and predict that 2D SnO_2 and PbO_2 exhibit the $1T$ structure. For 2D GeO_2, we predict a new monoclinic structure, as well as several other nearly degenerate structures. Their low formation energies ($<$ 151 meV/atom) and dynamic stability indicate that it should be possible to synthesize them as free standing layers or on substrates. We find that 2D SiO_2, GeO_2 and SnO_2 are insulators and 2D PbO_2 is a semiconductor. SiO_2 displays a direct gap, and the others indirect band gaps. The band edge alignments reveal that 2D SiO_2 can serve as a gate oxide material for single-layer MoS_2 and phosphorene, while the other 2D dioxides are suitable as type-II and type-III heterostructures for single-layer MoS_2 and phosphorene. An assessment of the dielectric properties and electrochemical stability of these 2D materials shows that 2D GeO_2 and SnO_2 are particularly promising candidates for gate oxides and SnO_2 also as a protective layer in nanoelectronic devices. The crystal structures, electronic band structures and Pourbaix diagrams of the 2D materials in this work can be found in our online database at `http://materialsweb.org`.[19]

ACKNOWLEDGMENTS

[1] H. L. Zhuang and R. G. Hennig, JOM **66**, 366 (2014).
[2] A. K. Singh, K. Mathew, H. L. Zhuang, and R. G. Hennig, J. Phys. Chem. Lett. **6**, 1087 (2015).
[3] B. C. Revard, W. W. Tipton, A. Yesypenko, and R. G. Hennig, Phys. Rev. B **93**, 054117 (2016).
[4] P. Miro, M. Audiffred, and T. Heine, Chem. Soc. Rev. **43**, 6537 (2014).
[5] Y. Sun, H. Cheng, S. Gao, Z. Sun, Q. Liu, Q. Liu, F. Lei, T. Yao, J. He, S. Wei, and Y. Xie, Angew. Chem. Int. Ed. **51**, 8727 (2012).
[6] H. L. Zhuang and R. G. Hennig, Phys. Rev. B **88**, 115314 (2013).
[7] K. F. Mak, C. Lee, J. Hone, J. Shan, and T. F. Heinz, Phys. Rev. Lett. **105**, 136805 (2010).
[8] A. Splendiani, L. Sun, Y. Zhang, T. Li, J. Kim, C. Chim, G. Galli, and F. Wang, Nano Lett. **10**, 1271 (2010).
[9] M. N. Blonsky, H. L. Zhuang, A. K. Singh, and R. G. Hennig, ACS Nano **9**, 9885 (2015).
[10] W. Wu, L. Wang, Y. Li, F. Zhang, L. Lin, S. Niu, D. Chenet, X. Zhang, Y. Hao, T. F. Heinz, and Z. L. Hone, James amd Wang, Nature **514**, 470 (2014).
[11] H. L. Zhuang, M. D. Johannes, M. N. Blonsky, and R. G. Hennig, Appl. Phys. Lett. **104**, 022116 (2014).
[12] K. Novoselov, D. Jiang, F. Schedin, T. Booth, V. Khotkevich, S. Morozov, and A. Geim, Proc. Nat. Acad. Sci. **102**, 10451 (2005).
[13] R. Mas-Balleste, C. Gomez-Navarro, J. Gomez-Herrero, and F. Zamora, Nanoscale **3**, 20 (2011).
[14] M. Xu, T. Liang, M. Shi, and H. Chen, Chem. Rev. **113**, 3766 (2013).
[15] H. L. Zhuang, A. K. Singh, and R. G. Hennig, Phys. Rev. B **87**, 165415 (2013).
[16] A. K. Singh, H. L. Zhuang, and R. G. Hennig, Phys. Rev. B **89**, 245431 (2014).
[17] A. K. Singh and R. G. Hennig, Appl. Phys. Lett. **105**, 051604 (2014).
[18] Z. Y. A. Balushi, K. Wang, R. K. Ghosh, R. A. Vila, S. M. Eichfeld, J. D. Caldwell, X. Qin, Y.-C. Lin, P. A. DeSario, G. Stone, S. Subramanian, D. F. Paul, R. M. Wallace, S. Datta, J. M. Redwing, and J. A. Robinson, Nature materials (2016).
[19] M. Ashton, J. Paul, S. B. Sinnott, and R. G. Hennig, Phys. Rev. Lett. **118**, 106101 (2017).
[20] L. Lichtenstein, C. Buechner, B. Yang, S. Shaikhutdinov, M. Heyde, M. Sierka, R. Wlodarczyk, J. Sauer, and H.-J. Freund, Ang. Chem. Int. Ed. **51**, 404 (2012).
[21] D. Löffler, J. J. Uhlrich, M. Baron, B. Yang, X. Yu, L. Lichtenstein, L. Heinke, C. Büchner, M. Heyde, S. Shaikhutdinov, H.-J. Freund, R. Włodarczyk, M. Sierka, and J. Sauer, Phys. Rev. Lett. **105**, 146104 (2010).
[22] P. Y. Huang, S. Kurasch, A. Srivastava, V. Skakalova, J. Kotakoski, A. V. Krasheninnikov, R. Hovden, Q. Mao, J. C. Meyer, J. Smet, D. A. Muller, and U. Kaiser, Nano Lett. **12**, 1081 (2012).
[23] W. W. Tipton and R. G. Hennig, J. Phys. Condens. Matter **25**, 495401 (2013).
[24] B. C. Revard, W. W. Tipton, and R. G. Hennig, in *Prediction and Calculation of Crystal Structures* (Springer, 2014) pp. 181–222.
[25] W. W. Tipton, C. R. Bealing, K. Mathew, and R. G. Hennig, Phys. Rev. B **87**, 184114 (2013).
[26] W. W. Tipton, C. A. Matulis, and R. G. Hennig, Comput. Mater. Sci. **93**, 133 (2014).
[27] Y. Le Page and G. Donnay, Acta Crystallogr. Sect. B **32**, 2456 (1976).
[28] A. A. Bolzan, C. Fong, B. Kennedy, and C. J. Howard, Acta Crystallogr. Sect. B **53**, 373 (1997).
[29] P. D'Antonio and A. Santoro, Acta Crystallogr. Sect. B **36**, 2394 (1980).
[30] G. Kresse and J. Hafner, Phys. Rev. B **47**, 558 (1993).
[31] G. Kresse and J. Hafner, Phys. Rev. B **49**, 14251 (1994).
[32] G. Kresse and J. Furthmller, Comp. Mater. Sci. **6**, 15 (1996).
[33] G. Kresse and J. Furthmüller, Phys. Rev. B **54**, 11169 (1996).
[34] P. E. Blöchl, Phys. Rev. B **50**, 17953 (1994).
[35] J. P. Perdew, K. Burke, and M. Ernzerhof, Phys. Rev. Lett. **77**, 3865 (1996).
[36] J. Heyd, G. E. Scuseria, and M. Ernzerhof, J. Chem. Phys. **118**, 8207 (2003).
[37] A. Togo, F. Oba, and I. Tanaka, Phys. Rev. B **78**, 134106 (2008).
[38] P. Y. Huang, S. Kurasch, A. Srivastava, V. Skakalova, J. Kotakoski, A. V. Krasheninnikov, R. Hovden, Q. Mao, J. C. Meyer, J. Smet, D. A. Muller, and U. Kaiser, Nano Lett. **12**, 1081 (2012).
[39] H. T. Stokes and D. M. Hatch, J. Appl. Crystallogr. **38**, 237 (2005).
[40] P. Rivero, J.-A. Yan, V. M. García-Suárez, J. Ferrer, and S. Barraza-Lopez, Phys. Rev. B **90**, 241408 (2014).
[41] A. K. Singh and R. G. Hennig, Appl. Phys. Lett. **105**, 042103 (2014).
[42] H. L. Zhuang and R. G. Hennig, Phys. Rev. B **88**, 115314 (2013).
[43] J. Heyd, J. E. Peralta, G. E. Scuseria, and R. L. Martin, J. Chem. Phys. **123**, 174101 (2005).
[44] W. Strehlow and E. Cook, J. Phys. Chem. Ref. Data **2**, 163 (1973).
[45] W. Mindt, J. Electrochem. Soc. **116**, 1076 (1969).
[46] F. Lappe, J. Phys. Chem. Solids **23**, 1563 (1962).
[47] J. Robertson, J. Vac. Sci. Technol. B **18**, 1785 (2000).
[48] D. Dragoman and M. Dragoman, *Advanced optoelectronic devices*, Vol. 1 (Springer Science & Business Media, 2013).
[49] I. Souza, J. Íñiguez, and D. Vanderbilt, Phys. Rev. Lett. **89**, 117602 (2002).
[50] A. H. Sihvola, *Electromagnetic mixing formulas and applications*, 47 (IET, 1999).
[51] J. C. Slater, J. Chem. Phys. **41**, 3199 (1964).
[52] G. H. Wannier, Phys. Rev. **52**, 191 (1937).
[53] D. R. Penn, Phys. Rev. **128**, 2093 (1962).

[54] K. Young and H. Frederikse, J. Phys. Chem. Ref. Data **2**, 313 (1973).

[55] D. Roessler and W. Albers, J. Phys. Chem. Solids **33**, 293 (1972).

[56] H. Van Daal, J. Appl. Phys. **39**, 4467 (1968).

[57] T. Minami, Semicond. Sci. Technol. **20**, S35 (2005).

[58] D. J. Payne, R. G. Egdell, D. S. Law, P.-A. Glans, T. Learmonth, K. E. Smith, J. Guo, A. Walsh, and G. W. Watson, J. Mater. Chem. **17**, 267 (2007).

[59] A. Beal and H. Hughes, J. Phys. C **12**, 881 (1979).

[60] T. Nagahama, M. Kobayashi, Y. Akahama, S. Endo, and S.-i. Narita, J. Phys. Soc. Jpn. **54**, 2096 (1985).

[61] S. M. Sze and K. K. Ng, *Physics of semiconductor devices* (Wiley, 2006).

[62] G. B. Alexander, W. M. Heston, and R. K. Iler, J. Phys. Chem. **58**, 453 (1954).

[63] P. M. Dove, N. Han, A. F. Wallace, and J. J. De Yoreo, Proc. Natl. Acad. Sci. **105**, 9903 (2008).